# Deuterated Water Effect in a Room Temperature Ionic Liquid: *N*,*N*-Diethyl-*N*-methyl-*N*-2-methoxyethyl Ammonium Tetrafluoroborate

**Hiroshi Abe,*,† Yusuke Imai,† Takahiro Takekiyo,‡ and Yukihiro Yoshimura‡**

*Department of Materials Science and Engineering and Department of Applied Chemistry, National Defense Academy, Yokosuka 239-8686, Japan*

*Received: November 18, 2009; Revised Manuscript Received: January 14, 2010*

A deuterated water effect in the room temperature ionic liquid (RTIL) *N*,*N*-diethyl-*N*-methyl-*N*-2-methoxyethyl ammonium tetrafluoroborate, [DEME][$BF_4$], is observed in its crystal domain structures; crystallization temperature, $T_c$; crystal superstructures; and volume contractions. The above effect, seen in [DEME][$BF_4$]−0.9 mol % $H_2O$ mixtures, is reduced in 1.0 mol % $0.75H_2O{\cdot}0.25D_2O$ and 0.9 mol % $0.5H_2O{\cdot}0.5D_2O$ mixtures and is completely suppressed in 1.3 mol % $D_2O$ mixtures. Interestingly, $T_c$ decreased systemically with D substitutions of water. In contrast to the crystal state, it was found that there is no difference between $H_2O$ and $D_2O$ mixtures in the liquid state, on the basis of X-ray diffraction patterns. At around 80−90 mol % $H_2O$, the intermolecular correlation of [DEME][$BF_4$] as a local structure changes to that of bulk water.

## 1. Introduction

A number of investigations on room temperature ionic liquids (RTILs) as potential green solvents have been made.[1] The curious nature of RTILs is represented by their almost zero vapor pressure. The chemical and thermal stability of RTILs prevents decomposition, even if RTILs are distilled at low pressure. In addition, electrochemical devices, such as an electric double layer capacitor, are being developed for industrial applications.[2]

Recently, *N*,*N*-diethyl-*N*-methyl-*N*-2-methoxyethyl ammonium tetrafluoroborate, [DEME][$BF_4$], as a different kind of RTIL was synthesized for electrochemical capacitors; it has quite a wide potential window.[2] The fundamental physical properties of [DEME][$BF_4$] were evaluated. In addition, anomalous domain growth was observed in the crystal structure of [DEME][$BF_4$]−$H_2O$ mixtures.[3] Here, three different types of domain structures were formed, even at a small content of $H_2O$. Twin-related domains appeared inside the conventional one at just 0.9 mol % $H_2O$. This anomalous domain growth was not seen in the mixtures of [DEME][$BF_4$]−$CH_3OH$, $C_2H_5OH$ or $C_6H_6$. Furthermore, two kinds of superstructures at 0.9 mol % $H_2O$ and 1.1 mol % $C_6H_6$ were determined.[4] Volume contraction of the unit cell occurred only in the above mixtures. By introducing a sublattice with an equivalent sublattice constant, the twin-related domains, two kinds of superstructures, and the volume contraction at 0.9 mol % $H_2O$ are well explained. A water network based on the sublattice was simulated and visualized using Monte Carlo simulation.[5] In addition, a complicated phase diagram in [DEME][$BF_4$]−$H_2O$ mixtures was determined by simultaneous X-ray diffraction and DSC measurements.[6,7] Below 4 mol % $H_2O$, a crystal phase (C-phase) is formed on cooling. An amorphous phase (A-phase) appears from 4 to 10 mol % $H_2O$. Above 10 mol %, a two-phase coexistence, (A + C)-phase, was observed. The pure A-phase is characterized by "two dynamic components" in its Raman spectra, in which the lower Raman band is crystal-like and the higher one is liquidlike. Quenched [DEME][$BF_4$]−$H_2O$ mixtures show a nearly free hydrogen bonded band (NFHB) of water in their Raman spectra,[8] where the water molecules do not interact with each other and are loosely bonded with $BF_4^-$ anions. This NFHB mode exists up to 80 mol % $H_2O$. In the [DEME][$BF_4$] system, density functional theory (DFT) calculations were carried out to determine the stable molecular conformations.[9] Only by considering two molecular conformations could the observed Raman bands be assigned consistently.

A "giant isotope effect" on hydrogen bonds is often seen in ferroelectric transitions. For instance, potassium dihydrogen phosphate ($KH_2PO_4$) and its deuterated compound ($KD_2PO_4$) have quite different phase transition temperatures, $T_c$. The $T_c$ of $KH_2PO_4$ is around 122 K, whereas that of $KD_2PO_4$ is 229 K. From DFT calculations,[10] the atomic positions of hydrogen are determined to be centered in the case of H (O−H−O) and off-center in the case of D (O···D−O). This centering can determine the bonding length, which is regarded as a geometrical effect. The distances between the oxygens, $d_{OO}$, are estimated to be 0.242 nm (H) and 0.251 nm (D), respectively. The quantum delocalization of the proton contributes to their attractive interaction, an effect known as "proton-mediated covalent bonding (PMCB)". As a geometrical effect, below $T_c$, the off-centering of the proton induces positional shifts of the P and K ions to stabilize the total energy. In further ab initio calculations of $KH_2PO_4$ and $KD_2PO_4$,[11] it was pointed out that proton motions are strongly correlated with the heavier ions within clusters, in addition to the geometrical effect. The feedback effect of the geometrical modifications can explain not only the isotope effect but also the phase transition under pressure. Further ab initio calculations introducing two different kinds of cluster models[12] suggest that rotational defects of $PO_4$ induce a lattice contraction in $KH_2PO_4$. The domain wall motion around the domain freezing temperature, $T_F$ (= $T_c$ − 60 °C), is influenced by polarization flip. Both the domain wall and polarization dynamics are controlled extensively by the proton motion.

H/D isotope effects relating to hydrogen bonding have drawn much attention in other branches, such as biophysics, for a long time.[13] Hydrogen-bond-mediated isotope effects are seen in bifurcated hydrogen bonds between interior-bound water mol-

* Corresponding author. E-mail: ab@nda.ac.jp.
† Department of Materials Science and Engineering.
‡ Department of Applied Chemistry.

10.1021/jp910947z 
Published on Web 02/10/2010

ecules and large proteins. In RTILs, the deuterated effect has not been discussed much so far, though various kinds of RTIL−water mixtures have been investigated experimentally and theoretically. Thus, our aim in this study is to clarify the deuterated water effect on a RTIL−water system. We have determined crystal structures of [DEME][$BF_4$]−$H_2O$, −0.75$H_2O$·0.25$D_2O$, −0.5$H_2O$·0.5$D_2O$ and −$D_2O$ mixtures by X-ray diffraction methods. Although no difference between $H_2O$ and $D_2O$ mixtures is seen in their liquid structures, their crystal domain structure, superstructures, volume contractions, and $T_c$ are strongly influenced by protonated water. PMCB in the crystals is much enhanced by a 1 mol % $H_2O$ mixture.

## 2. Experiments

We selected [DEME][$BF_4$] (Kanto Chemical Co.) as a RTIL. Since this RTIL is hydrophilic, 126 ppm $H_2O$ was included in the as-received sample (estimated on the basis of the Karl Fischer titration method). For addition to [DEME][$BF_4$], initial concentrations of $H_2O$ (0.9 mol %), 0.75$H_2O$·0.25$D_2O$ (1.0 mol %), 0.5$H_2O$·0.5$D_2O$ (0.9 mol %) and $D_2O$ (1.2 mol %) mixtures were prepared, although some extent of H−D exchange between $H_2O$ and $D_2O$ molecules is to be expected when mixed. For mixtures, we used distilled water, $H_2O$ (Wako Pure Chemical Co.) and $D_2O$ (Aldrich Co.). The sample solutions were prepared by dissolving [DEME][$BF_4$] in distilled water mixed with an appropriate fraction of $D_2O$. Special care was taken with the sample preparations, which were done in a drybox to avoid atmospheric $H_2O$.

At room temperature, X-ray diffraction patterns of the liquid state were measured using an 18 kW X-ray generator (RINT 2500, Rigaku Co.). Cu Kα radiation ($\lambda$ = 0.1542 nm) was selected for the incident X-ray. Scattered intensity was monochromated by curved highly oriented pyrolytic graphite (002). The transmission geometry of the sample was set to collect data. The thickness of the sample holder was 1 mm. The X-ray windows of the holder were polyimide thin films (Kapton), whose thickness was 7.5 $\mu$m. By using the step scan mode at fixed intervals, a few thousand counts were collected, even at high scattering angles for both the samples and background.

To analyze the X-ray diffraction patterns quantitatively (electron units per molecule), we measured several integrated intensities of a standard powdered sample of Ni.[14] The calculated Compton scattering was subtracted from the corrected X-ray diffraction patterns. Here, the scattering vector, $Q$, is defined to be $4\pi(\sin\theta)/\lambda$ (nm$^{-1}$). The radial distribution function (RDF) is given by[15,16]

$$4\pi r^2(\rho - \rho_0) = \frac{2r}{\pi z^2}\int_0^\infty Qi(Q)\sin(Qr)\,dQ \qquad (1)$$

$z^2$ is provided by $z^2 = \sum_n z_n^2$, where $z_n$ is the atomic number of the $n$th component atom.

In situ observations were performed using simultaneous X-ray diffraction and DSC measurements. The DSC was attached to a vertical goniometer with a 2 kW X-ray generator (RINT-Ultima III, Rigaku Co.). For in situ observations of the liquid state, a sample stage was fixed horizontally. A sealed X-ray tube and a scintillation counter moved simultaneously. A parallel beam was obtained using a parabolic multilayer mirror. A long soller slit was placed in front of the scintillation counter. Cu Kα radiation ($\lambda$ = 0.1542 nm) was selected for the simultaneous measurements. During simultaneous measurements, dry $N_2$ gas flowed at 20 cc/min to reduce moisture.

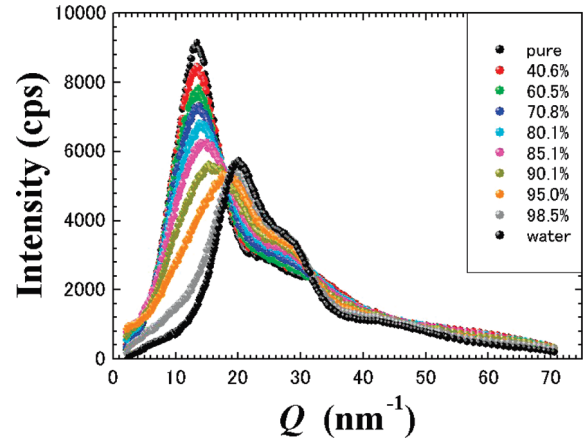


**Figure 1.** X-ray diffraction patterns in [DEME][$BF_4$]−$x$ mol % $H_2O$ mixtures at room temperature.

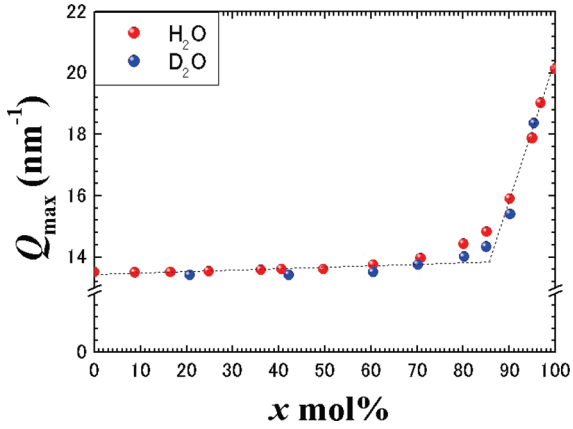


**Figure 2.** $H_2O$ and $D_2O$ concentration dependences of Q position at the maximum intensity, $Q_{max}$, of X-ray diffraction patterns (Figure 1). $Q_{max}$ values increase drastically above 90 mol % $H_2O$ and $D_2O$.

DFT calculations were used as the investigation methodology for the interactions between the RTILs and water molecules.[17,18] Here, we performed DFT calculations on the optimized arrangement of the $BF_4^-\cdots n(H_2O)$ ($n$ = 1−4, where $n$ is the number of $H_2O$) complexes to investigate the interaction between the $BF_4^-$ anions and water molecules. All DFT calculations were carried out using the Gaussian03 program.[19] For calculations on the $BF_4^-\cdots n(H_2O)$ complexes, we used Becke's three-parameter (B3) exchange function.[20] The B3 exchange function was combined with the Lee−Yang−Peer correlation function (B3LYP).[21] All calculations by this method were performed using the 6-311++G(d,p) basis set.

## 3. Results

**3.1. The Liquid State of [DEME][$BF_4$]−[$H_2O$] and [$D_2O$] Mixtures.** Figure 1 shows the X-ray diffraction patterns of [DEME][$BF_4$]−$x$ mol % $H_2O$ mixtures at room temperature. Around 80−90 mol %, the pattern changes drastically. To analyze the change as a function of water concentration, we calculated the $Q$ position at the maximum intensity, $Q_{max}$. Above 90 mol %, $Q_{max}$ shifts to higher values of $Q$. The same tendency of $Q_{max}$ is seen in [DEME][$BF_4$]−$D_2O$ mixtures. $Q_{max}$ as a function of $H_2O$ and $D_2O$ concentrations is plotted in Figure 2. At the same time, classical RDF analysis can evaluate local molecular correlations. For quantitative analysis, background and air scattering were first subtracted from the observed intensities, then X-ray absorption and polarization factors were corrected. After these fundamental corrections, the absolute

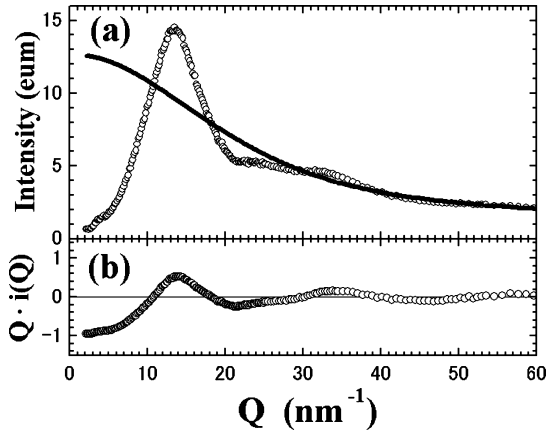


**Figure 3.** (a) X-ray diffraction intensity of pure [DEME][$BF_4$] in electron units per molecule. Solid curve reveals calculated $\sum_i\{f_i(Q)\}^2 + R\sum_i I_i^{comp}(Q)$. (b) Weighted structure function of pure [DEME][$BF_4$].

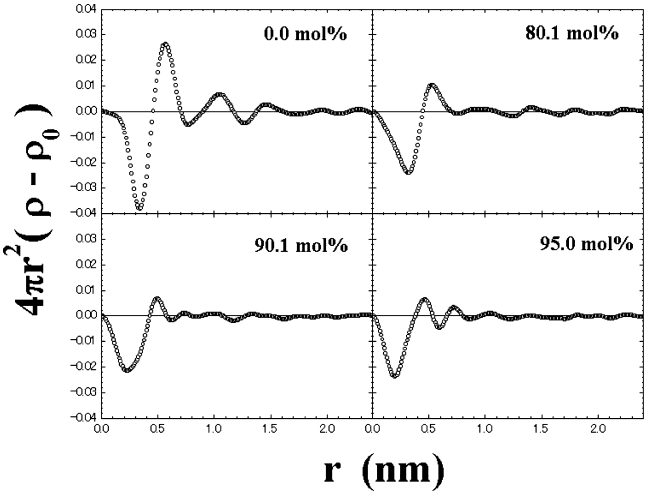


**Figure 4.** Radial distribution function of [DEME][$BF_4$]−$x$ mol % $H_2O$ mixtures. At 90 mol % $H_2O$ as a crossover point from the [DEME][$BF_4$] network to a bulk water one, molecular correlation visibly decreases.

value (electron units per molecule) was calculated from Bragg reflections of standard polycrystalline Ni. The calculated Compton scattering as incoherent scattering was removed from the corrected intensity. Then we could obtain the coherent intensity, $I^{coh}$. The open circles in Figure 3a show the $I^{coh}$ of pure [DEME][$BF_4$]. The square of the average atomic scattering factor per molecule, $\langle f^2\rangle$, is represented by the solid curve in Figure 3a. The oscillating component, $i$(Q), is provided by

$$i(Q) = \frac{I^{coh} - \langle f^2\rangle}{\langle f^2\rangle} \qquad (2)$$

The weighted structure function, $Qi(Q)$, is shown in Figure 3b. The RDF is calculated by inverse Fourier transform of $Qi(Q)$ in eq 1. The RDF of [DEME][$BF_4$]−$H_2O$ mixtures depends greatly on the $H_2O$ concentration, as shown in Figure 4. A pairwise interaction around 0.55 nm is notable in pure [DEME][$BF_4$]. With increasing water concentration, the correlation becomes weaker. At 90.1 mol % $H_2O$, the correlation has almost vanished. Above 90 mol %, a different kind of molecular correlation develops along with the rapid increase in $Q_{max}$.

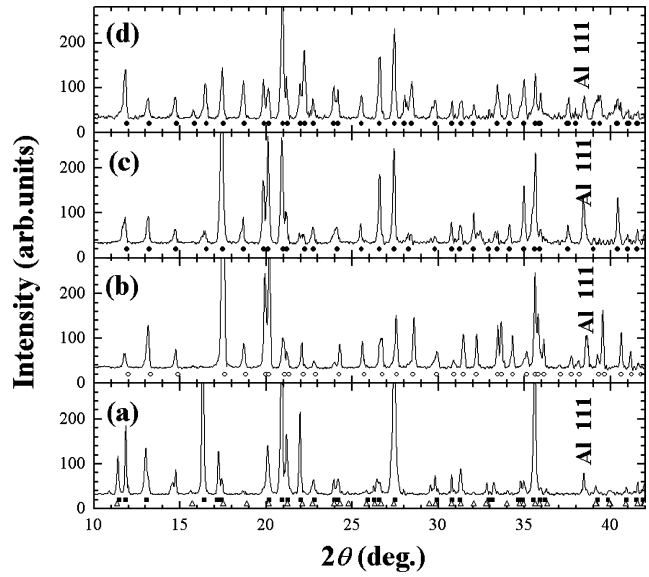


**Figure 5.** X-ray diffraction patterns at −80 °C of (a) [DEME]-[$BF_4$]−0.9 mol % $H_2O$, (b) −1.0 mol % 0.75$H_2O$·0.25$D_2O$, (c) −0.9 mol % 0.5$H_2O$·0.5$D_2O$, and (d) −1.3 mol % $D_2O$. Closed squares show the $a_O' \times b_O' \times 2c_O'$ modulated lattice, and open triangles show the $2a_O' \times b_O' \times 2c_O'$ modulated one. Open circles and closed circles are calculated positions of the orthorhombic lattices, $a_O' \times b_O' \times c_O'$ and $a_O \times b_O \times c_O$, respectively.

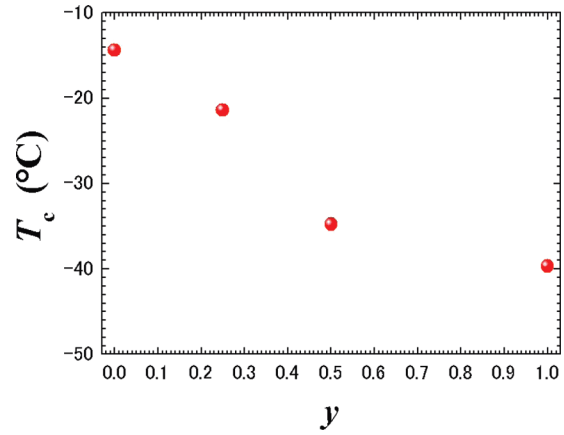


**Figure 6.** Crystallization temperature in 1 mol % (1−$y$)$H_2O$·$yD_2O$ mixtures. With increasing $y$, $T_c$ visibly decreases.

**3.2. Crystallization of [DEME][$BF_4$]−[(1 − $y$)$H_2O$·$yD_2O$] Mixtures.** Crystal structures of [DEME][$BF_4$]−0.9 mol % $H_2O$, −1.0 mol % 0.75$H_2O$·0.25$D_2O$, −0.9 mol % 0.5$H_2O$·0.5$D_2O$, and −1.3 mol % $D_2O$ were determined by X-ray diffraction methods. Figure 5a−d shows the diffraction patterns of [DEME]-[$BF_4$]−0.9 mol % $H_2O$, −1.0 mol % 0.75$H_2O$·0.25$D_2O$, −0.9 mol % 0.5$H_2O$·0.5$D_2O$, and −1.3 mol % $D_2O$ at −80 °C, respectively. Here, the crystallization temperature, $T_c$, is determined precisely by simultaneous X-ray and DSC measurements.[3] First, to show the deuterated water effect, we provide the crystallization temperature, $T_c$, in 1 mol % (1 − $y$)$H_2O$·$yD_2O$ mixtures as a function of $y$, in Figure 6. It is obvious that $T_c$ decreases with increasing D substitution. Then, $2\theta$ values of Bragg reflections were fitted well to an orthorhombus ($\Delta 2\theta <$ 0.2° ($2\theta <$ 20°); $\Delta 2\theta <$ 0.1°, (20° < $2\theta$)). Superstructures represented by $a_O' \times b_O' \times 2c_O'$ (closed squares) and $2a_O' \times b_O' \times 2c_O'$ (open triangles) are shown in Figure 5a. $a_O'$, $b_O'$, and $c_O'$ are smaller than the normal orthorhombic lattice, $a_O$, $b_O$, and $c_O$.[4] The modulated lattices are not detected in −1.0 mol % 0.75$H_2O$·0.25$D_2O$, −0.9 mol % 0.5$H_2O$·0.5$D_2O$, or

**TABLE 1: Crystallization Temperatures, $T_c$, Unit Cells of Crystal Structures and Volume Per Four Molecules ($Z = 4$), $V_4$, of [DEME][$BF_4$]−0.9 mol % $H_2O$, −1.0 mol % 0.75$H_2O$·0.25$D_2O$, −0.9 mol % 0.5$H_2O$·0.5$D_2O$, and −1.3 mol % $D_2O$**

| | $H_2O$ | | 0.75$H_2O$·0.25$D_2O$ | 0.5$H_2O$·0.5$D_2O$ | $D_2O$ |
|---|---|---|---|---|---|
| $x$ (mol %) | 0.9 | | 1.0 | 0.9 | 1.3 |
| $T_c$ (°C) | −14.4 | | −21.4 | −34.8 | −39.7 |
| unit cell | $a_O' \times b_O' \times 2c_O'$ | $2a_O' \times b_O' \times 2c_O'$ | $a_O' \times b_O' \times c_O'$ | $a_O \times b_O \times c_O$ | $a_O \times b_O \times c_O$ |
| $V_4$ (nm$^3$) | 1.145 | 1.101 | 1.181 | 1.212 | 1.209 |

−1.3 mol % $D_2O$ if the content of $D_2O$ increases. $T_c$, unit cells, and their volumes are summarized in Table 1.

In addition to X-ray diffraction patterns ($\theta-2\theta$ scan mode), crystal domain structures were examined by the $\theta$ scan mode, where the $\theta$ scan mode (rocking curve) is perpendicular to the $\theta-2\theta$ scan mode in the reciprocal lattice. Figure 7a−d reveals the rocking curves on the Debye rings of the [DEME][$BF_4$]−0.9 mol % $H_2O$, −1.0 mol % 0.75$H_2O$·0.25$D_2O$, −0.9 mol % 0.5$H_2O$·0.5$D_2O$, and −1.3 mol % $D_2O$ mixtures, respectively. The rocking curves were obtained at a fixed $2\theta$ value (27.4°). In the case of [DEME][$BF_4$]−0.9 mol % $H_2O$ and −1.0 mol % 0.75$H_2O$·0.25$D_2O$ solutions, a highly preferred orientation appears extraordinary on the Debye ring (Figure 7a−b). Judging from the asymmetric peak profiles or two peak tops, each sharp component consists of a pair of peaks. The full width at half-maximum (fwhm) of the peaks is estimated to be around 0.2°, where the mosaicity is equivalent to that of a single crystal, whereas in the 0.9 mol % 0.5$H_2O$·0.5$D_2O$ solution, a conventional preferred orientation is observed. Weak intensity modulations on the Debye ring are expressed by much broader and weaker peaks. Interestingly, the preferred orientation disappears completely in 1.3 mol % $D_2O$ solutions. Instead, randomly orientated microdomains are effected by the deuterated effect of water.

## 4. Discussion

**4.1. Protonated and Deuterated Effect on Crystallization.** At first, we focus on the H/D effect in the crystal as shown in Figures 5 and 7. On the basis of the idea of the protonated effect in $KH_2PO_4$,[12] we assume the hydrogen bonding in the solid, from a microscopic perspective, is as follows: (i) As already stated in the introduction, NFHB typically appears in the OH-stretching Raman spectra of the solutions. In slow-cooled solids, the water molecules that participate in NFHB in the liquid state might be bound to the F of the anion and also the O of the large cation, as shown in Figure 8a. Due to the highly packed solid structure, PMCB (H−O−H) is employed. (ii) D in the solid stays in its off-centered position (O···D−O), as shown in Figure 8b. Where there is PMCB (hydrogen delocalization) in the crystal, the atomic distance between O and O, $d_{OO}$, becomes shorter (Figure 8a), but this attractive interaction does not occur in deuterated water, since the deuteron is stabilized in the off-center position as with $KD_2PO_4$. From assumption ii, it follows that associating with deuterated water leads to a larger $d_{OO}$. We imply that the PMCB in the [DEME][$BF_4$]−0.9 mol % $H_2O$ crystal causes an extraordinary volume contraction, partly seen in the results in Table 1. A large contribution from PMCB in 1.0 mol % 0.75$H_2O$·0.25$D_2O$ also provides a small volume contraction.

As for macroscopic H/D effects, we discuss whether the anomalous domain structure as shown in Figure 7 originates from the H/D effect. Generally, twin-related domains are caused by an elastic property over a long range. On the other hand, the present results show that the H/D effect is based on a microscopic perturbation. Despite the difference in scale, domain formations are influenced by the H/D effect. Similarly, the $T_c$ in Figure 6, although a macroscopic property, is connected with the H/D effect. However, the dynamic process connecting the microscopic to the macroscopic still remains unclear. Certainly, it is not sufficient to describe the dynamic motion of the domain wall by X-ray diffraction alone. Dynamic properties relating to its local structure could be interpreted from Raman data, but there is further difficulty in detection in such a small content of water. In fact, we could not detect the differences due to the H/D effect in the Raman spectra at 1 mol % water.

**4.2. No Protonated or Deuterated Effect in Liquid.** Alternatively, by characterizing the liquid state precisely, the peculiar features of the H/D effect on crystal structure would be clarified. Recently, many studies of the liquid state of RTILs have been carried out by experiments and theoretical simulations. For instance, the liquid structure of [$C_2$mim][TFSI] (1-ethyl-3-methylimidazolium bis-(trifluoromethanesulfonyl)imide) has been investigated by X-ray diffraction, $^1$H, $^{13}$C and $^{19}$F NMR, and molecular dynamics (MD) simulations.[22] Here, a series of

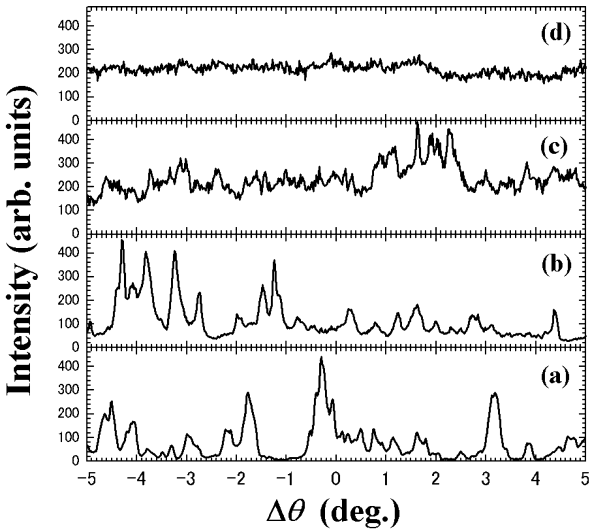


**Figure 7.** Rocking curves at −80 °C of (a) [DEME][$BF_4$]−0.9 mol % $H_2O$, (b) −1.0 mol % 0.75$H_2O$·0.25$D_2O$, (c) −0.9 mol % 0.5$H_2O$·0.5$D_2O$, and (d) −1.3 mol % $D_2O$.

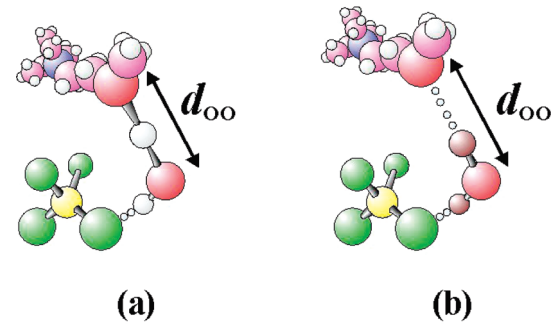


**Figure 8.** A bonding scheme of (a) $H_2O$ and (b) $D_2O$ in crystal. In protonated water, "on-centering" is preferred, whereas "off-centering" occurs in deuterated water. The atomic distance between oxygens, $d_{OO}$, varies depending on the interaction.

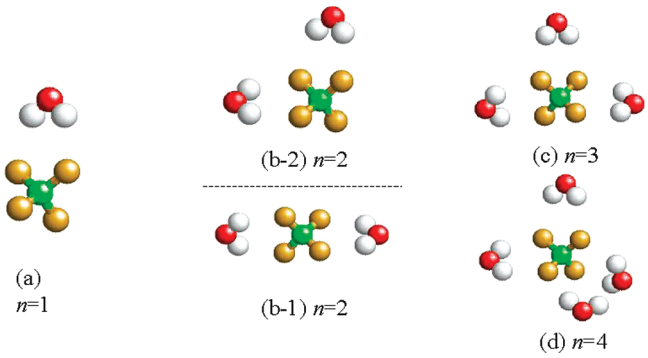


**Figure 9.** Optimized structures of the $BF_4^-$—$n(H_2O)$ ($n$ = 1−4) complex using the B3LYP/6-311++G(d,p) basis set. Green, brown, gray, and red represent the boron, fluorine, hydrogen, and oxygen atoms. In the case of the $BF_4^-$−$2H_2O$ complex, the $BF_4^-$ anion takes two arrangement patterns with two water molecules; one is a linear arrangement (b-1) and another is a perpendicular arrangement (b-2). The former is energetically more stable than the latter ($\Delta E$ = 1.6 kJ/mol).

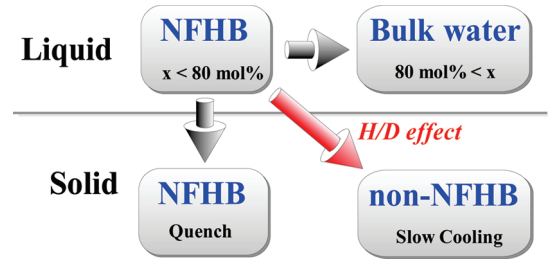


**Figure 10.** Nearly free hydrogen bond band of water mapping in the liquid and solid states. NFHB is selectively observed in the Raman spectra, where NFHB reveals the OH oscillator which does not form a hydrogen bonding network among water molecules, as in pure bulk water.

cations, such as 1-alkyl-3-methyl imidazolium are described as [$C_n$mim] using the alkyl chain length, $n$. MD simulations including intra- and intermolecular interactions were carried out referring to the experimentally obtained RDF. In particular, the partial RDF is sensitive to molecular conformations. The simulation results are consistent with NMR experiments. In a mixed system, RDF analysis provides significant insight despite the much more complicated interactions among molecules. In [$C_1$mim][$PF_6$]−benzene mixtures, the benzene concentration dependence of packing efficiency was elucidated by neutron diffraction methods.[23] The mixing effect of benzene addition causes repulsive interactions between cation and cation. It was figured out that benzene can dissolve homogeneously into [$C_1$mim][$PF_6$].

By introducing the following assumption, we can discuss the curious liquid state obtained from the RDF analysis of [DEME][$BF_4$]−$H_2O$ (and also $D_2O$ mixtures) as shown in Figure 4: One $BF_4^-$ anion can interact loosely with four water molecules through weak H···F bonding without forming a bulk water network in the liquid state. If we take into account fully connected F ($BF_4$−water = 1:4), it is natural that bulk water tends not to appear at $x$ < 80 mol %. This idea gives rise to an isolated $BF_4$−water cluster, which is surrounded by large cations. To prove this assumption, we carried out DFT calculations[9] on the optimized arrangements of the $BF_4^-$···$n(H_2O)$ complexes using the B3LYP/6-311++G(d,p) basis set.

A series of molecular arrangements between $BF_4^-$ and $H_2O$ are illustrated in Figure 9. As pointed out above, H···F bonding is realized in the simulation box. The optimized arrangements as shown in Figure 9 are in good agreement with the maximum number ($n$ = 4) (∼80 mol %) of water molecules bonded to each $BF_4^-$ anion. In the $BF_4^-$···$n(H_2O)$ ($n$ > 4) complexes (>80 mol %), non-H···F bonded water molecules appear, since each $BF_4^-$ anion is fully connected with four $H_2O$ molecules. The optimized arrangements can explain well the observed Raman modes in the liquid state.[24] This assumption is also supported by the critical crossover point in the X-ray diffraction, in which quite a large change of local circumstance was detected around 80−90 mol % water. The RDF, like the molecular correlations, changes from [DEME][$BF_4$]-like to bulk-water-like at the critical concentration.

From the viewpoint of H/D effects in the liquid state, the local structure as a function of water concentration does not depend on $H_2O$ or $D_2O$. Compared with the periodic molecular arrangement in the crystal, the bonding length between F (an anion) and O (water) is longer in the liquid state, and a $BF_4$−water cluster with longer bonding should exist in the liquid state with some lifetime. Due to the dynamic nature of the $BF_4$−water clusters in the liquid state, the PMCB seen in crystals did not appear in the liquid. Consequently, we think that the H/D effect is not detected in the local structure in the liquid state of [DEME][$BF_4$]−water mixtures on the basis of X-ray diffraction patterns.

**4.3. Liquid Structures with Nearly Free Hydrogen Bonding.** In previous studies, we have shown that there exists NFHB in the Raman spectra of liquid and solid [DEME][$BF_4$]−water mixtures.[7,8] Here, we try to view our results in conjunction with the NFHB scheme. (a) NFHB in the OH or OD stretching mode is observed up to 80 mol % water in the Raman spectrum. (b) By slow cooling, the NFHB of water disappears when it is solidified. The experimental results previously obtained from Raman are summarized in Figure 10. In result a, a picture of loosely aggregated $BF_4$−water clusters corresponds to the OH stretching mode in the Raman spectrum; one OH of the water molecule is loosely bonded to the F anion, whereas the other OH, facing the large cations, becomes free. Result b suggests that the bonding scheme is drastically modified in the crystal state. That is, the nearly free state of OH or OD in the liquid state is forced to bind to a cation under a periodic order due to packing effects in the crystal. This is proved by the lack of a NFHB band in the crystal. From the "NFHB mapping", we can see that NFHB is consistent with our earlier assumption about the intermolecular bonding.

We insist that the NFHB of water is a clue to resolving the 1.0 mol % $H_2O$ anomalies in the crystal structure. Bonding nature as well as molecular conformations[9] are also important. For further understanding of the PMCB induced by protonated water, DFT calculations of the [DEME][$BF_4$]−$D_2O$ system are needed, and these are in progress.

## 5. Summary

In the liquid structure, an original correlation in [DEME][$BF_4$] is sustained up to 80 mol % $H_2O$. We point out that NFHB is observed within the same region of water concentration. It is stressed that nearly free hydrogen bonding can exist even in the water-rich region. Theoretically, it has also been proved that $BF_4^-$−$n(H_2O)$ clustering is preferred, according to DFT calculations. Intermolecular interactions represented by weak H···F bonding prevent the formation of a bulk water network. $D_2O$ mixtures show almost the same water concentration dependence.

On the other hand, a H/D effect occurs extensively in crystallization. Composite domain structure, superstructures and volume contractions at 0.9 mol % $H_2O$ are suppressed by D

substitution of water. A scenario of PMCB and slow proton motion as in hydrogen-bonded $KH_2PO_4$, is key to interpreting the above anomalies in the [DEME][$BF_4$]−0.9 mol % $H_2O$ mixture, although the cause of the decrease of $T_c$ inversely proportional to D substitution remains unclear. As normally expected in the case of the $KH_2PO_4$−$KD_2PO_4$ system, the $T_c$ of the deuterated compound is much higher.

**Acknowledgment.** We appreciate Ms. M. Yasaka and Mr. A. Kishi of Rigaku Co. for their experimental support and helpful discussions. The authors also thank Professor H. Matsumoto and Professor T. Arai of the National Defense Academy for helpful discussions.

## References and Notes

(1) Earle, M. J.; Seddon, K. R. *Pure Appl. Chem.* **2000**, *72*, 1391. Cooper, E. R.; Andrews, C. D.; Wheatley, P. S.; Webb, P. B.; Wormald, P.; Morris, R. E. *Nature* **2004**, *430*, 101. Earle, M. J.; Esperanca, J. M. S. S.; Gilea, M. A.; Lopes, J. N. C.; Rebelo, L. P. N.; Magee, J. W.; Seddon, K. R.; Widegren, J. A. *Nature* **2006**, *439*, 831.

(2) Sato, T.; Masuda, G.; Takagi, K. *Electrochim. Acta* **2004**, *49*, 3603.

(3) Imai, Y.; Abe, H.; Goto, T.; Yoshimura, Y.; Kushiyama, S.; Matsumoto, H. *J. Phys. Chem. B* **2008**, *112*, 9841.

(4) Imai, Y.; Abe, H.; Yoshimura, Y. *J. Phys. Chem. B* **2009**, *113*, 2013.

(5) Abe, H.; Imai, Y.; Goto, T.; Yoshimura, Y.; Aono, M.; Takekiyo, T.; Matsumoto, H.; Arai, T. *Metal. Mater. Trans. A* **2009**, in press.

(6) Imai, Y.; Abe, H.; Goto, T.; Yoshimura, Y.; Michishita, Y.; Matsumoto, H. *Chem. Phys.* **2008**, *352*, 224.

(7) Abe, H.; Yoshimura, Y.; Imai, Y.; Goto, T.; Matsumoto, H. *J. Mol. Liq.* **2009**, *150*, 16.

(8) Yoshimura, Y.; Goto, T.; Abe, H.; Imai, Y. *J. Phys. Chem. B* **2009**, *113*, 8091.

(9) Takekiyo, T.; Imai, Y.; Abe, H.; Yoshimura, Y. in preparation.

(10) Koval, S.; Kohanoff, J.; Migoni, R. L.; Tosatti, E. *Phys. Rev. Lett.* **2002**, *89*, 187602.

(11) Koval, S.; Kohanoff, J.; Lasave, J.; Colizzi, G.; Migoni, R. L. *Phys. Rev. B* **2005**, *71*, 184102.

(12) Lasave, J.; Koval, S.; Dalal, N. S.; Migoni, R. L. *Phys. Rev. B* **2005**, *72*, 104104.

(13) Liu, A.; Lu, Z.; Wang, J.; Yao, L.; Li, Y.; Yan, H. *J. Am. Chem. Soc.* **2008**, *130*, 2428.

(14) Abe, H.; Yamamoto, K.; Matsuoka, S.; Matsuo, Y. *J. Phys.: Condens. Matter* **2007**, *19*, 466201.

(15) Nishikawa, K.; Iijima, T. *Bull. Chem. Soc. Jpn.* **1984**, *57*, 1750.

(16) Katayanagi, H.; Hayashi, S.; Hamaguchi, H.; Nishikawa, K. *Chem. Phys. Lett.* **2004**, *392*, 460.

(17) Zhang, L.; Xu, Z.; Wang, Y.; Li, H. *J. Phys. Chem. B* **2008**, *112*, 6411.

(18) Danten, Y.; Cabaco, M. I.; Besnard, M. *J. Mol. Liq.*, in press.

(19) Frish, M. J.; Trucks, G. W.; Schlegel, H. B.; Scuseria, G. E.; Robb, M. A.; Cheeseman, J. R.; Zakrzewski, V. G.; Montogomery, J. A.; Daniels, A. D.; Kudin, K. N.; Strain, M. C.; Farkas, O.; Tomasi, J.; Barone, V.; Cossi, M.; Cammi, R.; Mennucci, B.; Pomelli, C.; Adamo, C.; Clifford, S.; Ochterski, J. W.; Petersson, G. A.; Ayala, P. Y., Cui, Q.; Morokuma, K.; Malick, D. K.; Rabuck, A. D.; Raghavechari, K.; Foresman, J. B.; Cioslowski, J.; Ortiz, J. V.; Baboul, A. G.; Stefanov, B. B.; Liu, G.; Liashenko, A.; Piskorz, P.; Komaromi, I.; Gomperts, R.; Martin, R. L.; Fox, D. J.; Keith, T.; Al-Laham, M. A.; Peng, C. Y.; Nanayaakkara, A.; Gonzalez, C.; Challacombe, M. P.; Gill, M. W.; Johnson, B.; Chen, W.; Wong, M. W.; Andres, J. L.; Gonzalez, C.; Head-Gordon, M.; Replogle, E. S.; Pople, J. A. *GAUSSIAN 03*, Gaussian, Inc.: Pittsburgh, PA, 2003.

(20) Becke, A. D. *Phys. Rev. A* **1998**, *38*, 3098.

(21) Lee, C.; Yang, W.; Parr, R. G. *Phys. Rev. B* **1998**, *37*, 785.

(22) Fujii, K.; Soejima, Y.; Kyoshoin, Y.; Fukuda, S.; Kanzaki, R.; Umebayashi, Y.; Yamaguchi, T.; Ishiguro, S.; Takamuku, T. *J. Phys. Chem. B* **2008**, *112*, 4329.

(23) Deetlefs, M.; Hardacre, C.; Nieuwenhuyzen, M.; Sheppard, O.; Soper, A. K. *J. Phys. Chem. B* **2005**, *109*, 1593.

(24) Takekiyo T.; Yoshimura, Y.; Imai, Y.; Abe, H. In preparation.

JP910947Z